Dynamic Response of Stereoblock Elastomeric Polypropylene Studied by Rheooptics and X-ray Scattering. 2. Orthogonally Oriented Crystalline Chains

Willy Wiyatno,[†] John A. Pople,[‡] Alice P. Gast,[§] Robert M. Waymouth,*,[⊥] and Gerald G. Fuller*,[†]

Chemical Engineering Department, Stanford University, Stanford, California 94305; Stanford Synchrotron Radiation Laboratory, Stanford Linear Accelerator Center, Stanford University, Stanford, California 94309; Chemical Engineering Department, Massachusetts Institute of Technology, Cambridge, Massachusetts 02139; and Department of Chemistry, Stanford University, Stanford, California 94305

ABSTRACT: A combination of tensile stress, rheooptical birefringence, and wide-angle X-ray scattering (WAXS) was used to probe the dynamic response of the low-tacticity ether-soluble (ES) fraction of elastomeric polypropylene (ePP) derived from metallocene 2-arylindene hafnium catalyst. The ES fraction has isotactic pentad distribution [mmmm] = 21% and a very low amount of crystallinity ($\leq$2% by differential scanning calorimetry and WAXS). In tensile stretching and step-strain shearing, ES exhibits unusual deformation behavior of crystalline chains preferentially oriented orthogonal relative to the deformation axis. Under deformation, WAXS shows arcing along the meridian axis at a scattering angle $2\theta = 16.0°$ ($d = 0.551 \pm 0.002$ nm) which coincides with one of the characteristic reflections of the β-form, but the higher order reflection for the β-form at $2\theta = 21.3°$ is not observed. The meridional arcing, which signifies crystallization of the low-tacticity fraction of ePP, is also observed when ES is blended with higher-tacticity fractions of ePP. The meridional arcing, however, is observed at $2\theta = 14.0°$, corresponding to (110) reflection of the α-form, instead of at $2\theta = 16.0°$ for the neat ES. The crystallization in the α-form offers evidence of cocrystallization of the ES fraction with the higher-tacticity components in the same crystalline form as the host matrix. We believe that the cocrystallization occurs through an epitaxial growth in the *ac*-faces of the α-form.

Introduction

The commercial importance of isotactic polypropylenes (i-PP) has driven numerous studies on the polymer synthesis, structure−property relationship, morphology, and rheological properties.[1−3] Crystallographic and morphological studies have shown that i-PP adopts a 3_1 or 3_2 helical conformation in the crystalline phase whether it is crystallized from melt or solution. Depending on the crystallization conditions, the helical chains can pack in various crystallographic unit cell structures. Three crystalline forms of i-PP are known, α-, β-, and γ-form, along with the mesomorphic form with a degree of ordering intermediate between the amorphous and crystalline phase.[2−5] Common processing operations, including film blowing, blow molding, injection molding, and fiber spinning, subject molten polymers to shear and elongational flow fields. The flow conditions influence the nucleation and crystallization behavior of the polymers and strongly affect the final morphology, physical, and rheological properties.[6]

Many studies have focused on the crystallization behavior of molten i-PP subjected to various flow fields.[7−10] Processing properties such as applied shear (or elongation) rate, strain, thermal condition, and duration sensitively influence the final morphology of i-PP. In the early 1990s, Janeschitz-Kriegl and co-workers devised an experimental method to investigate the effect of short-term intense shearing of isothermal polymer melt on subsequent crystallization.[7] The formation of shish-kebab structures in intermittent shear flows of i-PP melts was observed. Subsequently, Janeschitz-Kriegl and co-workers reported that the growth speed of the oblong particles is larger in the transverse direction.[11] The transverse oblong structures were also observed on slightly undercooled melt of high molar mass high-density polyethylene (HDPE) continuously sheared at low shear rates.[12] Recently, Kornfield et al. investigated the short-term shearing effect on the structure and morphology of crystallizing i-PP with wide-angle X-ray scattering (WAXS), in situ optical birefringence, and ex situ microscopy using a newly developed experimental apparatus.[13−15] They discovered that highly oriented fiberlike crystallites developed within "shish-kebab" morphology, with lamellae (kebabs) growing on the nuclei (shish) until they impinged upon one another. Hsiao et al. have studied aspects of crystallization behavior of i-PP in various conditions.[16−20] Crystalline phase transformation from the α-form to the mesomophic form was found at low temperatures in drawn i-PP fibers. Varga and Karger-Kocsis have reported shear-induced crystallization of the β-form which was nucleated from the α-form row nuclei of polypropylenes at 135 °C.[21−23] Transcrystalline-like superstructures were formed by stretching a glass fiber embedded in a polypropylene matrix studied by polarized optical microscopy together with scanning electron (SEM) and atomic force microscopy (AFM). The presence of the α-form row nuclei was demonstrated by selective melting (166 °C) of the β-form crystallites, having a

[†] Chemical Engineering Department, Stanford University.
[‡] Stanford Linear Accelerator Center, Stanford University.
[§] Massachusetts Institute of Technology.
[⊥] Department of Chemistry, Stanford University.

Table 1. Polymer Characterization

							crystallinity%	
sample	M_w [a] $(\times 10^{-3})$	PDI[a]	mmmm (%)[b]	m (%)[b]	T_m (°C)[c]	ΔH (J/g)[c]	DSC	XRD
ePP-10	201	2.3	34	73	42−149	22	11	8
ES-ePP10	147	2.1	21	67	41−45	2	1	2
HI-ePP10	432	2.5	76	92	47−155	82	39	37
blend ES/HI			34	72				
atactic PP	375	2.2	9	58				

[a] Determined by GPC (Waters, 150 °C) at BP Chemical Co. [b] Determined by ^{13}C NMR. [c] Determined by DSC endotherm scan from 0 to 200 °C at 20 °C/min.

lower melting temperature than the α-form crystallites.

The numerous studies on isotactic PP have enhanced our understanding of the structure, morphology, and the processing properties of the material. Recent advances in catalyst technology have made available a variety of low-density polypropylenes that exhibit elastomeric properties. The potential commercial applications of elastomeric polypropylenes (ePP) have driven a number of studies in the past few years.[24−37] Our group has shown that metallocene catalysts derived from 2-aryl-indene ligands produced elastomeric polypropylenes.[38−41] Polypropylenes produced with this class of catalysts have narrow molecular weight distributions and low levels of crystallinity. Despite its low crystallinity, morphological studies have revealed crystalline structures reminiscent of classical semicrystalline polymers, showing lamellae organizing into hedrites and spherulites.[42] In part 1 of the series, we have investigated the dynamic response and the origin of tensile set of ePP and its solvent fractions. Crystalline phase transformation from the α-form to the mesomorphic form was observed, originating from the intermediate- and high-tacticity fractions. The low-tacticity fraction contained chains in the crystalline domains that preferentially oriented orthogonal relative to the deformation axis.

In this second part of the series, we examine the unusual deformation behavior of the low-tacticity ether-soluble fraction (ES). A combination of tensile stress, rheooptical birefringence, and wide-angle X-ray scattering (WAXS) was used to probe the material's response under uniaxial tensile and step-shear deformations. The thermal stability of the crystallites containing polymer chains oriented orthogonally was examined. Furthermore, a blend of ES with the high-tacticity fraction of ePP was also studied. The ES/HI blend investigation allowed an assessment of the mechanism of the crystallization of ES in the presence of α-form crystallites.

Experimental Section

Materials. Elastomeric polypropylene ePP-10 was prepared at BP Chemical Co. by metallocene catalyst bis(2-(3,5-di-*tert*-butylphenyl)indenyl)hafnium dichloride with MAO as cocatalyst at 50 °C in liquid propylene.[43] The ether-soluble fraction (ES) was obtained by boiling-solvent extraction of the ePP-10 in diethyl ether as reported in part 1. Subsequent extraction of the ether-insoluble portion in heptane resulted in a heptane-soluble (HS) fraction of an intermediate tacticity and a heptane-insoluble (HI) fraction of a high tacticity. Table 1 shows the material characterization. The ES/HI blend was obtained by physical blending of the ES and HI fractions to match the tacticity of the ePP, [mmmm] = 34%. ES and HI fractions, with a weight ratio of 3.17, were dissolved in boiling xylene under N_2 atmosphere and subsequently dried in a vacuum. Atactic polypropylene (a-PP) was synthesized by bis-(2-phenylindenyl)hafnium dichloride catalyst at 75 psig at 20 °C, as previously reported.[44] GPC analysis showed the atactic
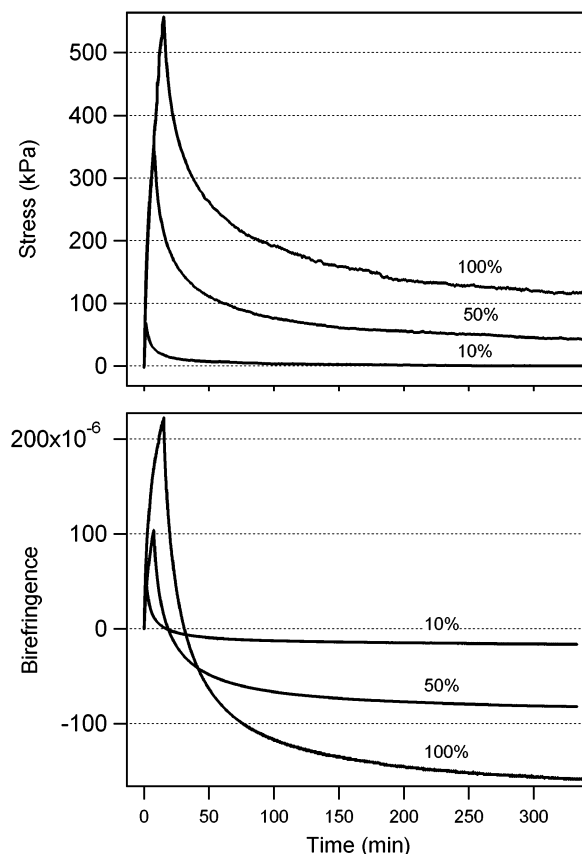

Figure 1. Simultaneous tensile stress and birefringence of ES at various strains. Specimens were elongated at 1 mm/min and held under strain after reaching the specified strain.

PP has M_w = 375K and M_w/M_n = 2.2. ^{13}C NMR showed an average pentad distribution [mmmm] = 9%.

Experimental Methods. Experimental procedures for tensile stress, dynamic birefringence, and WAXS have been reported in part 1. Tensile stretching was carried out with a Material Tester, MiniMat 2000 (Rheometric Scientific, Inc.), at room temperature using ASTM D-1708 dumbbell specimens with a gauge length of 2.2 cm. Crosshead separation rate for elongation and contraction was 1.0 and 0.1 mm/min, respectively. True tensile stress (σ) was calculated as the ratio of tensile force (F) to the instantaneous cross-sectional area (A) interpolated from caliper measurements: $\epsilon = F/A$. Strain (ε) was computed from the ratio of the change in separation distance (Δl) between two lines drawn at the middle of the specimen to its original separation distance (l_0): $\epsilon = \Delta l/l_0$.

Rheooptics dynamics birefringence was used to investigate the orientation dynamics of the materials.[45] Polarized monochromatic HeNe light (632.8 nm) was used as the light source in a setup whose schematic is shown in Figure 1 of part 1. WAXS was performed at beamline 1-4 of Stanford Synchrotron Radiation Laboratory (SSRL) with a flux ∼10^{10} photons at a wavelength of λ = 1.488 Å. The scattering vector (q) follows the relationship $q = (4\pi/\lambda) \sin(\theta)$, where λ is the scattering wavelength and θ is the scattering angle. The scattering data

are presented in terms of an equivalent 2θ for a wavelength of $\lambda = 1.54$ Å.

Step-strain shear deformations were performed in a Linkam shear cell (CSS-450) equipped with a temperature controller. The sample was sandwiched between two parallel glass-windows adjusted to a thickness of 500 μm, with the light beam traveling along the shear gradient axis. Step-strain deformation was carried out by a clockwise displacement of the bottom window at a shear rate of 100 s^{-1}. For reversible step-strain experiments, a reversed step-strain was applied at a later time with a counterclockwise displacement of the bottom window. All materials followed the same pre-thermal treatment before data were taken. Polymers were heated to melt (180 °C) for 10 min to erase all prior thermal history, cooled to the desired temperature at 20 °C/min, and annealed for 1 day.

Results

Simultaneous Tensile Stress–Birefringence. Figure 1 contains the results of simultaneous tensile stress and birefringence of the low-tacticity ES fraction at various strains. Dog-bone specimens, cut according to ASTM D-1708 (gauge length 2.2 cm), were stretched by a Minimat Tensile stretcher at 1 mm/min. During stretching, both the tensile stress and birefringence rose to positive values. Since polypropylene has a positive stress–optical coefficient, positive birefringence denoted net average chains orientation parallel to the strain direction.[46,47] Once the specified strain was reached, the specimen was held at strain to follow the in situ relaxation dynamics of the tensile stress and birefringence. Stress relaxed to positive plateaus whose values increased with increasing strain. The birefringence, on the other hand, unexpectedly relaxed to negative plateaus whose absolute values increased with increasing strain. The negative birefringence implied a net average chain orientation orthogonal to the strain axis following the polymer relaxation. Thus, stress relaxation transformed the net average chain orientation from a parallel to an orthogonal direction with respect to the deformation axis.

The results of a control experiment (simultaneous stress–birefringence) of an atactic polypropylene (a-PP) with isotacticity [mmmm] = 9% are shown in Figure 2. The validity of the stress–optical law for an amorphous polypropylene was confirmed. Stretching the sample to 25% yielded positive values of the stress and birefringence, similar to those seen in the ES. During stress relaxation, both the stress and birefringence decreased toward zero, with values mapping each other. Upon releasing from stress, the birefringence again tracked the stress very well. The measured stress–optical coefficient (SOC) of a-PP was 0.85 × 10^{-9} Pa^{-1}, in agreement with values reported in the literature.[46,48]

Figure 3 contains the data of simultaneous stress–birefringence of Figure 1 plotted as birefringence vs stress with time as an implicit parameter. During stretching, the birefringence followed a linear response with stress, especially at low strains. The slope yielded an apparent stress–optical coefficient (SOC) of 0.5 × 10^{-9} Pa^{-1}, which was 40% smaller than that of the atactic PP. The smaller SOC indicated there was a negative contribution to the birefringence as ES underwent deformation. At higher strains, the birefringence exhibited negative deviation relative to those at low strains; this could be attributed to the more negative birefringence contribution at higher strains. The "terminal" values of the relaxed stress and birefringence, after 6 h relaxation, followed a linear dependence with strains within the strain range studied.
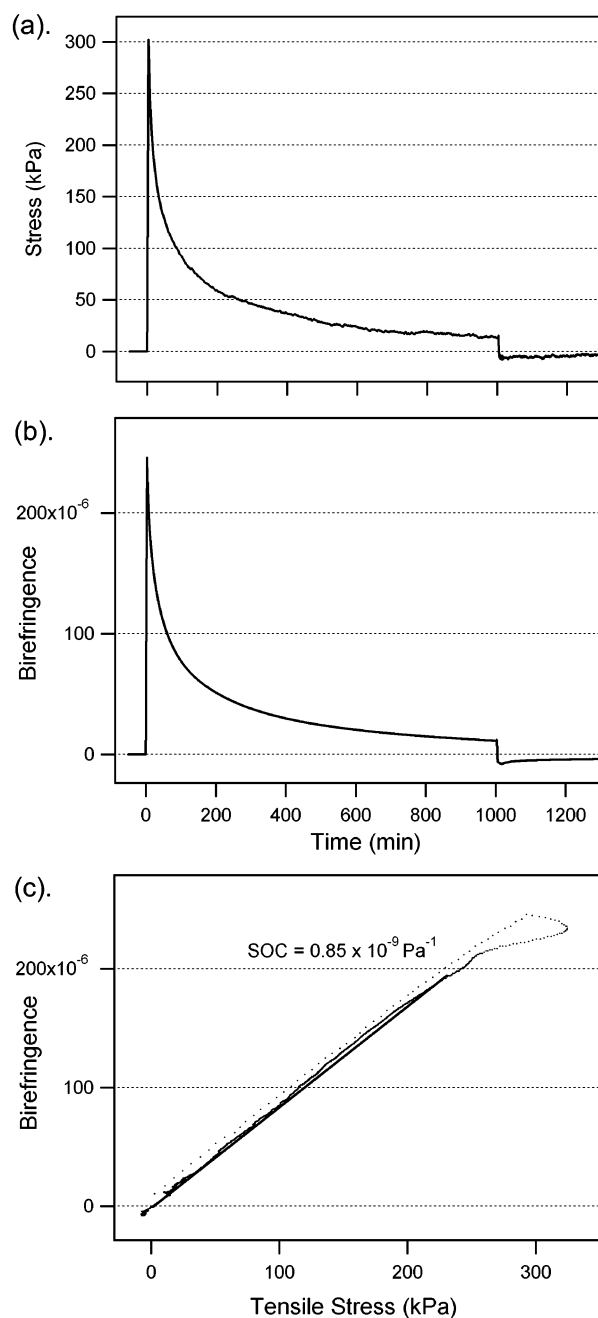

Figure 2. Response of atactic polypropylene subjected to uniaxial tensile extension of 25% strain: (a) simultaneous tensile stress and birefringence results; (b) the stress–optical law.

The reversibility of the negative birefringence was examined by monitoring the birefringence after the sample was released from stress (Figure 4). A dog-bone specimen was elongated to 50% and held for 14 h, after which it was released from stress. After 14 h relaxation at zero stress, a residual birefringence of -0.7×10^{-4} was detected. Compared to the plateau value of -1.05×10^{-4} when the sample was held under 50% strain, the residual permanent birefringence decreased 35% in absolute value. This indicated that the elements contributing to the negative birefringence were able to partially relax after being free from strain.

To examine whether the negative birefringence response arose uniquely from uniaxial extensional deformations, step-shear experiments were carried out in a Linkam shear cell equipped with a temperature control-
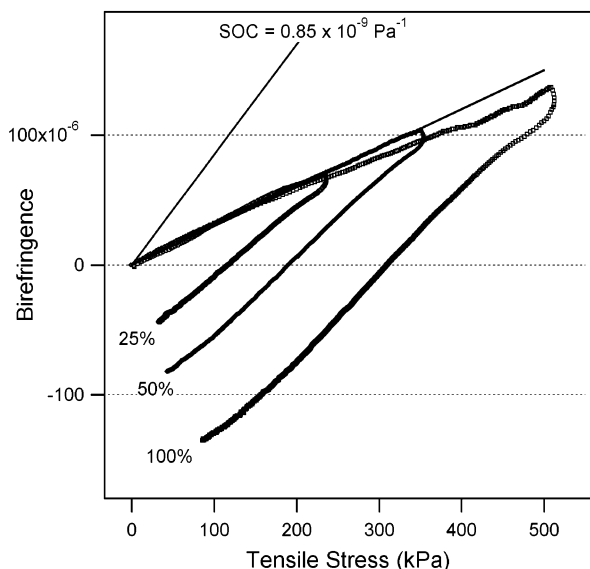
Figure 3. Simultaneous tensile stress and birefringence response of ES presented in the form of birefringence−stress curves. The upward curves show the stretching response while the downward curves correspond to 6 h stress relaxation.
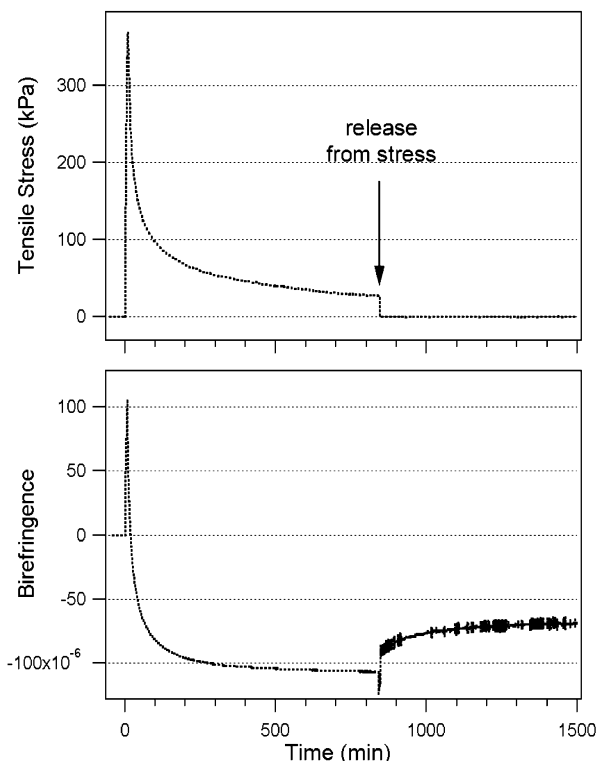

Figure 4. Residual birefringence of ES subjected to tensile stretching. Sample was initially subjected to 50% strain and held for 14 h to follow the relaxation dynamics. The sample was then free from strain, and the residual birefringence was monitored.

ler. At room temperature, the birefringence response following a 250% step-shear was positive. Similar to that seen in tensile stretching, the birefringence also yielded negative values during stress relaxation as displayed in Figure 5. Thermal investigation of the unusual negative birefringence was carried out by heating the sheared sample at 5 °C/min. The birefringence became more positive (tended toward zero) with increasing temperature and reached zero near 75 °C and remained zero with increasing temperatures. This suggested that

the negative birefringence arose from negatively bire-fringent crystallites, which completely melted at approximately 75 °C. The negatively birefringent crystallites were quite thermally stable below 35 °C, where the birefringence increased slowly with increasing temperature. Above 60 °C, the crystallites melted rapidly during heating with a sharp increase in birefringence.

To further investigate the thermal stability of the negatively birefringent crystalline phase, reversible step-shear experiments were performed at 50 and 80 °C, as shown in Figure 5c−d. At 50 °C, below the melting temperature of the crystallites, a 250% clockwise step-shear resulted in negative birefringence. After 1 h relaxation, a 250% counterclockwise step-shear showed an almost complete birefringence recovery. The slight negative birefringence might be attributed to the crystallites' inability to relax completely. Conducting the same experiments at 80 °C, a temperature above the crystalline melting point, yielded a radically different behavior. Step-shear deformations in both directions resulted in a complete birefringence relaxation that indicated a complete melting of the negatively birefringent crystallites at this temperature.

WAXS. A complementary wide-angle X-ray scattering was carried out to probe the unusual deformation properties of ES. Figure 6 contains 2-D WAXS images prior to stretching and at 300% strain. The unstretched ES exhibited a scattering halo typical of an amorphous material. Stretching the ES caused scattering arc to develop along the meridian axis that indicated the presence of crystalline domains with chains preferentially oriented orthogonal relative to the strain direction. The perpendicular chain orientation was in agreement with the observed negative birefringence.

The level of molecular anisotropy was monitored with 1-D azimuthal intensity profiles shown in Figure 7. The azimuthal plots integrated the scattering intensity over a narrow annulus centered at the meridional crystalline arc ($15.2° \leq 2\theta \leq 16.8°$). Unstretched ES had a flat azimuthal intensity profile, implying an isotropic chain orientation. At 100%, meridional arc developed with a width of approximately 110° (55° at both sides of the arc). At higher strain, the peak intensity increased and the width of the meridional arc became narrower, suggesting a more well-ordered chain orientation at higher deformations. At 300%, the arc width decreased to approximately 80°, which was 30° smaller than that at 100% strain. The specimen held at 300% for 1 h did not show appreciable change in the meridional arc. This suggested that no crystalline relaxation occurred within the experimental time scale.

Intensity scattering profiles (1-D) as a function of scattering angle 2θ along the meridian axis are shown in Figure 7, averaged over 40° (±20° within the meridional axis) for each strain. The unstretched sample showed a typical scattering profile of an amorphous polymer with a small scattering peak centered at $2\theta = 16.3°$ ($d = 0.542 \pm 0.003$ nm). As the sample was stretched, a scattering peak centered at $2\theta = 16.0°$ ($d = 0.551 \pm 0.002$ nm) appeared, suggesting a crystallization induced by stretching. The crystalline arc became wider (thicker) with increasing strain. Releasing the sample from stress (after 1 h at 300%) resulted in an almost complete relaxation, revealing reversible oriented crystalline domains. The percent crystallinity as a function of deformation, measured as area of the crystalline peak normalized by the total scattering area
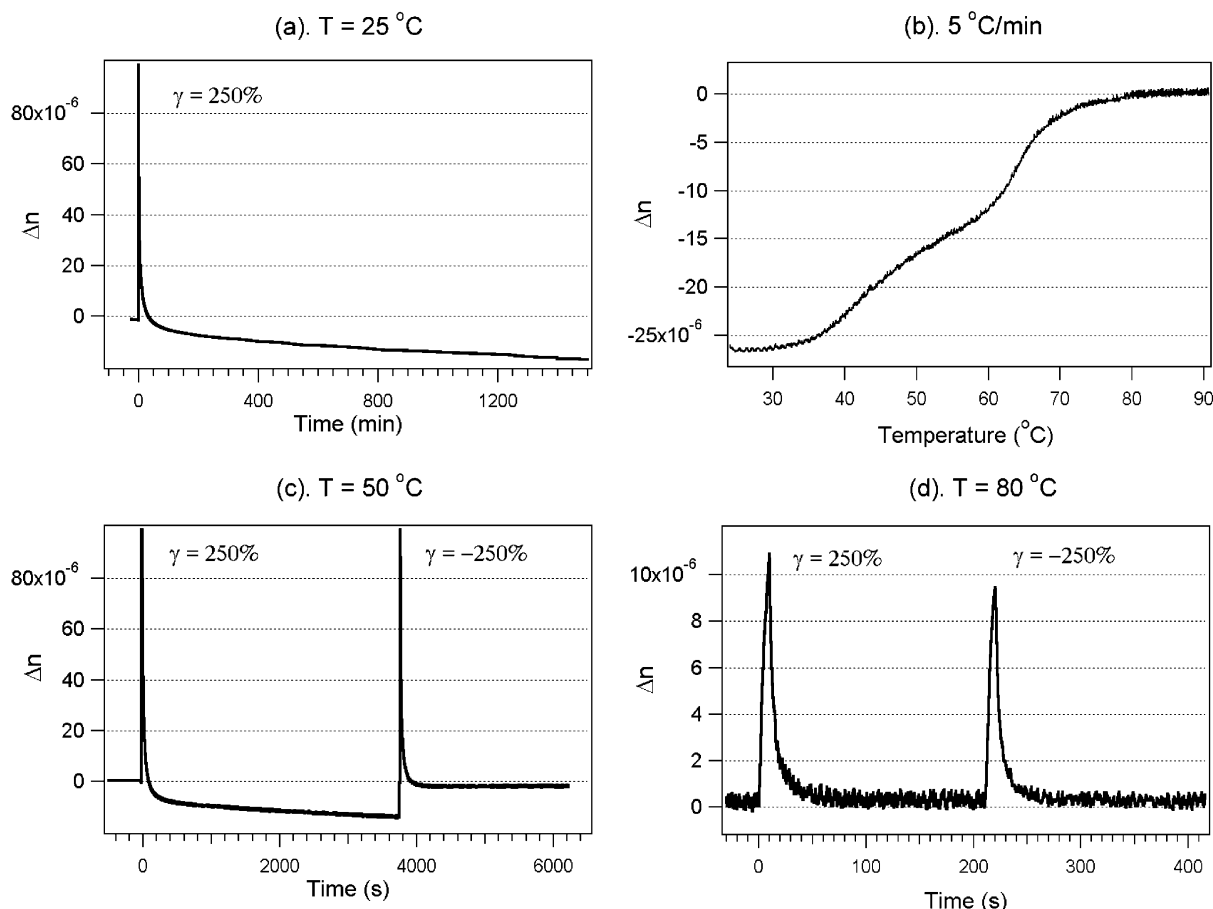
Figure 5. Birefringence response of ES under step-shear deformations: (a) step-shear at 25 °C; (b) under 250% strain from part (a), heat at 5 °C/min; (c) reverse step-shear at 50 °C; and (d) reverse step-shear at 80 °C .

(including the amorphous contribution), yielded crystallinity of 0.5% prior to stretching, 3.6% at 300%, and 0.6% upon the release of stress.

ES/HI Blend. The role of ES in an α-form crystalline matrix was examined with an ES/HI blend, prepared to match the isotacticity [mmmm] of ePP. WAXS showed that an undeformed ES/HI blend exhibited crystalline scattering peaks reminiscent of the α-form isotactic PP, like those of ePP and its higher tacticity fractions (Figure 8).[2,3] Upon stretching, three sets of scatterings appeared: meridional arc at $2\theta = 14.0°$, weak diffuse hump along the equatorial axis, and off-axis diagonal scattering at $2\theta = 21.5°$. Compared to the results of neat HI fraction as shown in Figure 9 of part 1, the meridional arc was greatly enhanced in the stretched ES/HI blend. Hence, the presence of the low-tacticity ES fraction in the ES/HI blend unambiguously led to an increase in the meridional arc. In the ES/HI blend, however, the meridional arcs occurred at $2\theta = 14.0°$, corresponding to the (110) reflections of the α-form rather than at $2\theta = 16.0°$ found in the neat ES. The meridian arc at the same scattering angle ($2\theta = 14.0°$) was also observed in the whole ePP containing the ES fraction.

The other scatterings in ES/HI blend were analogous to those found in the neat HI and in the whole ePP: the weak diffuse hump along the equatorial axis and the off-axis diagonal scatterings. As previously discussed in part 1, these scatterings corresponded to chains oriented parallel relative to the strain axis and a crystalline phase transformation from the α-form to the mesomorphic form. Crystalline phase transformation resulted

from chains pulling from their α-form crystallites (or its defects) to a less-ordered arrangement with random helical hand registration.[3,17,49−51] High deformation caused chains in the crystallites to orient along the strain axis and ruptured the crystalline form.

Figure 9 contains WAXS 1-D intensity scattering profiles of ES/HI blend reduced from the 2-D patterns presented in Figure 8. The azimuthal profiles, integrated over the (110) reflection at $13.4° \leq 2\theta \leq 14.6°$, exhibited two sets of scattering peaks. Scattering peaks centered at 90° and 270° were analogous to those observed in the neat ES fraction and ePP, whereas those centered at 0° and 180° were typical of the HI fraction. As expected, the scattering peaks increased with increasing strain. Interestingly, the meridian scattering peaks persisted to high deformations, up to 300% strain. The observed sets of scattering peaks differed in their relative intensity and sharpness. The ES peaks were broad and had a higher intensity than those of the HI fraction. Higher deformation caused narrowing of the ES peaks in the same qualitative manner as in the neat ES. Upon releasing from stress, some residual anisotropy was observed. Compared to the results of the neat HI fraction that exhibited plastic deformation, the ES/HI blend showed some relaxation.

Scattering intensity profiles along the meridian axis across a 40° span (20° on each side of the axis) are presented in Figure 9. As mentioned above, the ES/HI blend crystallized in the α-form isotactic PP. An increase in crystallinity originated from the ES chains was clearly seen as the intensity of the (110) reflection of the α-form increased with increasing strain. Other
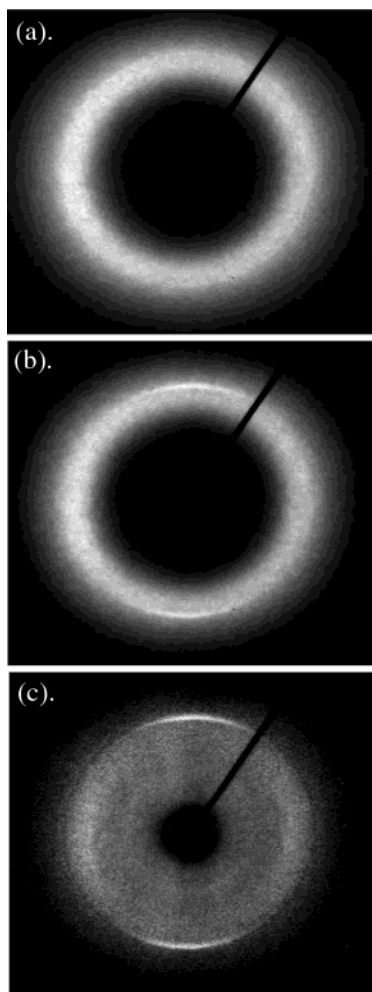
Figure 6. 2-D WAXS patterns of ES with strain axis along the vertical direction: (a) unstretched, (b) at 300% strain, and (c) at 300% strain after subtraction of the unstretched scattering pattern.

scattering peaks, the (040) and (130) reflections, did not exhibit an increase in intensity with increasing strain. Hence, the increase crystallinity could be unambiguously ascribed to the ES chains crystallizing in the (110) crystallographic packing of the α-form. Moreover, the deformation also caused the α-form meridional crystalline peaks to shift to lower scattering angles, indicative of the formation of larger *d*-spacings within the sample. Assuming a chain-folding packing of chains within lamellae, the shift in peaks along the meridian originated from chains oriented orthogonal to the strain axis, of which the lamellae were aligned parallel to the strain axis. The larger *d*-spacing implied that the chains oriented orthogonal to the strain axis (within lamellae) became more loosely packed under deformation. When the sample was released from stress, the scattering reflections returned to their original positions, and the intensity of the (110) reflection reduced to that before deformation. This suggested some reversibility of the crystalline deformation.

Discussion

The dynamic response of the low-crystallinity ES fraction of ePP-10 to tensile and shear deformations is unusual. Application of a tensile or shear deformation leads to an initial orientation parallel to the strain direction, as evidenced by the positive birefringence.

When held under strain, the values of both stress and birefringence decrease due to chain relaxation. The birefringence, however, decreases unexpectedly to negative values (Figures 1 and 5). The change in the sign of birefringence implies that a net chain orientation is transformed from parallel to orthogonal direction to the strain direction during stress relaxation. The thermal stability of the negative birefringence, up to approximately 75 °C (Figure 5), and the WAXS meridional arc (Figure 6) imply that the negative birefringence originates from chains in the crystalline domains. During stress relaxation, the crystalline chains dominate the birefringence to result in negative values.

Orientation of Amorphous and Crystalline Chains. The change in sign of the ES birefringence, from positive to negative, during stress relaxation indicates that the net chain orientation is shifted 90° when held under strain. This unusual phenomenon can be understood from the origin of the total birefringence. We believe that the tensile or shear deformation leads to two birefringence contributions, arising from amorphous and crystalline chains. The amorphous chains, oriented parallel to the deformation axis, yield positive birefringence (Figures 1 and 5). The crystalline chains, induced by deformation, contain negative birefringence as their net average chain orientation is orthogonal to the deformation direction. The detected total birefringence is a net of the two contributions. The initial positive birefringence signifies that the amorphous chain contribution dominates over the negative crystalline contribution. During stress relaxation, the amorphous chains are able to relax from their highly aligned state, while the negatively birefringent crystallites experience little or no relaxation. Hence, at a long time scale, the crystalline birefringence dominates the overall birefringence, resulting in what appears to be a shift in the net chain orientation.

The change in sign of birefringence can also be explained by deconvoluting the total birefringence to amorphous and crystalline contributions. Using an appropriate stress−optical coefficient (SOC), the amorphous contribution of birefringence can be extracted from the tensile stress data. The SOC of atactic PP (0.85×10^{-9} Pa^{-1}) was used to extract the "amorphous" birefringence contribution, by multiplying the SOC with the tensile stress (Figure 1). This approach assumes that tensile stress is derived entirely from the oriented amorphous chains as in atactic polypropylene. As shown in Figure 10, this analysis reveals that both amorphous and crystalline birefringence grow during deformation, with positive and negative contributions, respectively. During deformation and in the early period of stress relaxation, the amorphous chains have larger positive birefringence than the crystalline birefringence, resulting in a total positive birefringence. During stress relaxation, the positive birefringence originating from amorphous chains diminishes faster, resulting in a net negative birefringence.

Orthogonally Oriented Crystalline Chains. Both the negative birefringence and WAXS meridional arc in both the neat ES and ES/HI blend offer unambiguous evidence of crystalline chains preferentially oriented orthogonal relative to the deformation axis. On average, the lamellae giving rise to the meridional arc are oriented parallel to the deformation axis with the crystalline chains packed in a chain-folding mechanism. In the ES/HI blend, the increase of the meridional
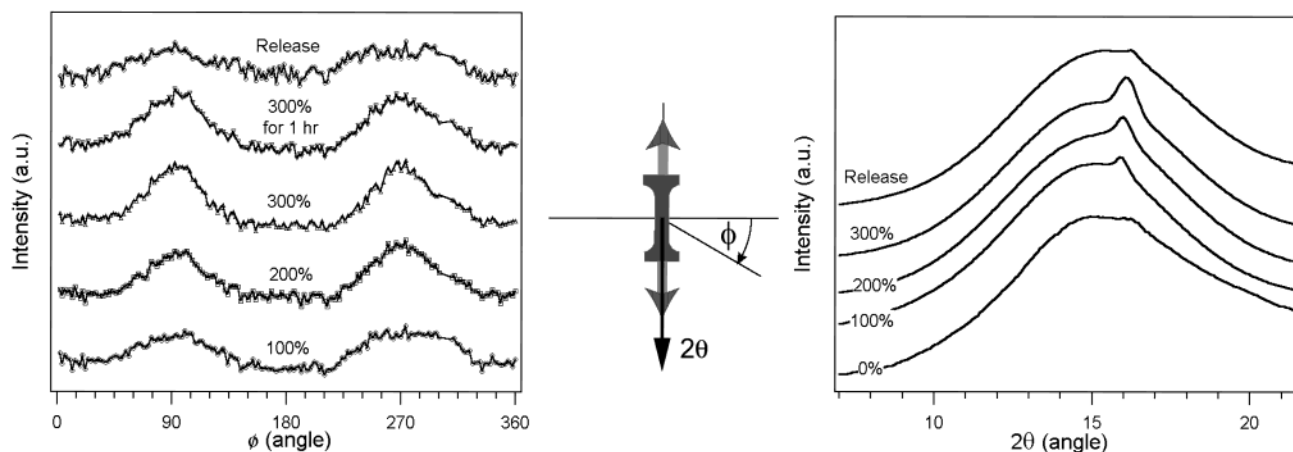
Figure 7. 1-D scattering profiles of ES at various strains: (a) azimuthal intensity plots integrated through an annulus of the meridional arcs; (b) intensity profiles along the meridional axis. Curves have been shifted along the *y*-axis for clarity.
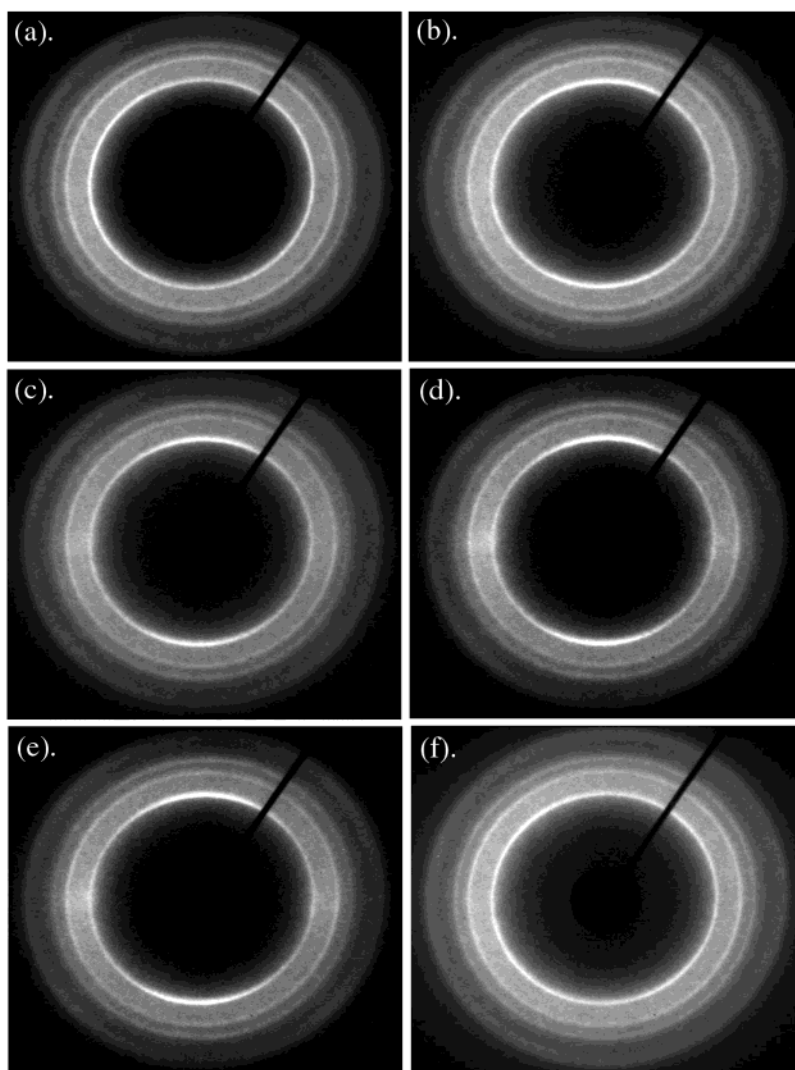

Figure 8. 2-D WAXS patterns of the ES/HI blend: (a) unstretched, (b) at 100% strain, (c) at 200%, (d) at 300%, (e) at 300% after 1 h relaxation, and (f) after 1 day free of 300% strain for 1 h.

arcing can be confidently attributed to the ES fraction as the neat HI fraction shows only weak meridional arcing as reported in part 1.

The orthogonally oriented crystalline chains can be understood in terms of two limiting cases: lamellae reorientation or deformation-induced crystallization. In one scenario, the crystalline domains (lamellae) are simply reoriented in the presence of a stress field. Morphological studies by AFM have shown that neat ES contains lamellae-type crystallites.[42,52] The lamellae are short and often blocklike or curved presumably due to frequent imperfections and/or shorter isotactic sequences. Deformation causes the lamellae to orient parallel to the strain axis; the low crystallinity of the
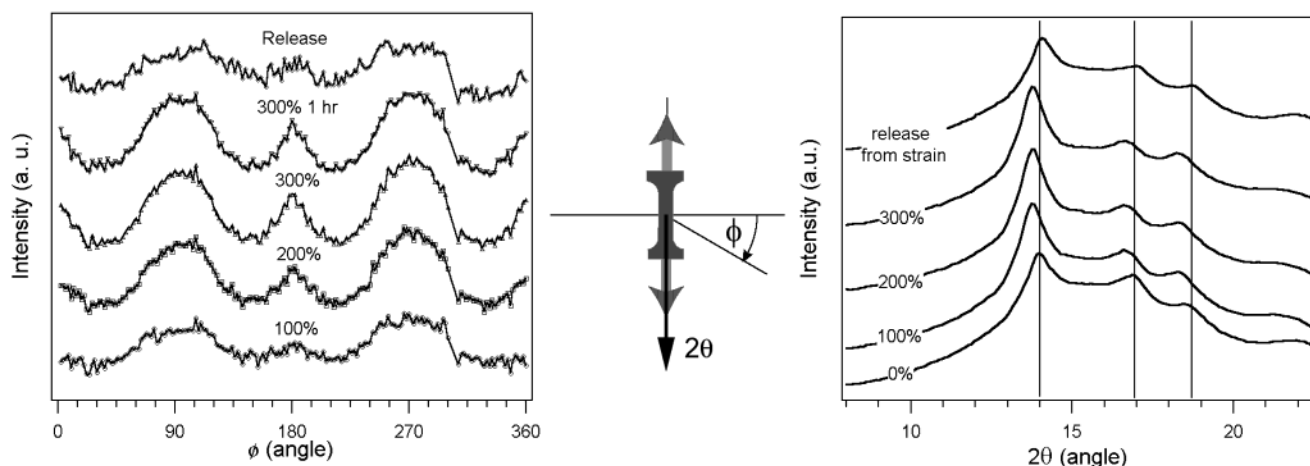
Figure 9. 1-D WAXS profiles of the ES/HI blend in tensile stretching at various strains: (a) azimuthal intensity plots of the (110) scattering peak; (b) intensity profiles along the meridional axis. Curves have been shifted vertically for clarity.
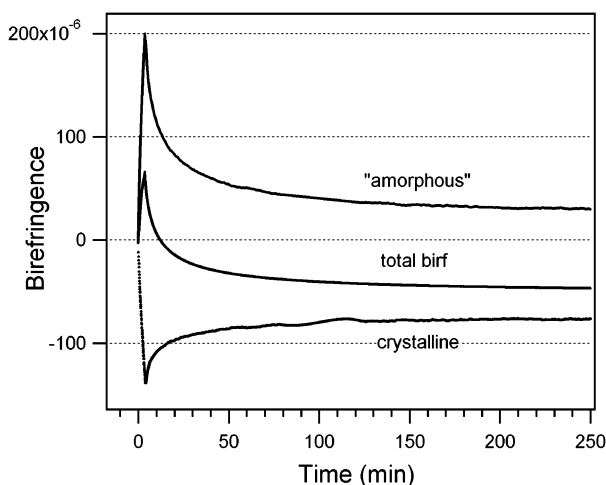

Figure 10. Crystalline and amorphous contributions of the birefringence of ES subjected to 25% step-shear deformation.

material provides mobility for the crystalline domains to undergo reorientation. The chains within the lamellae are oriented orthogonal to the long axis of the lamellae (chain folding) so the individual molecules are on average aligned orthogonal to the strain axis. Another limiting scenario is where the orthogonally oriented crystalline chains are formed through deformation-induced crystallization of the ES chains. An external stress causes the ES chains to diffuse to nucleation sites to form crystallites. The chains within lamellae are arranged orthogonal to the strain axis; the lamellae, induced by deformation, are preferentially aligned parallel to the deformation direction.

The deformation response, observed by WAXS, of the ES fraction by itself and when it is blended with higher-tacticity fractions (in ES/HI blend and ePP) provides insight into the deformation mechanism of the crystalline phase. WAXS of the deformed neat ES exhibits arc along the meridian at $2\theta = 16.0°$ (Figures 6 and 7). In samples containing the ES fraction, such as in ES/HI blend and ePP, the meridional arc is not present at $2\theta = 16.0°$ but instead it occurs at the (110) reflection of the α-form corresponding to $2\theta = 14.0°$ (Figures 8 and 9). Higher-order crystalline reflections of the α-form in ES/HI blend and ePP, the (040) and (130) reflections, do not exhibit meridional arc. The arc at the (110) reflection and the absence of crystalline arc at $2\theta = 16.0°$ provide evidence of cocrystallization of the ES chains

with the α-form crystallites. The absence of meridional arc at (040) and (130) reflections implies that the ES chains are predominantly arranged in the crystalline domains according to the observed scattering plane of the (110) reflection. If the cocrystallization of the ES chains were to occur homogeneously throughout the α-form crystalline phase, arcing would have occurred at other scattering reflections as well.

The observed crystallization of the ES fraction implies that long crystallizable sequences are present in the low-tacticity ES with isotacticity [mmmm] = 21%. The crystallization of ES chains is remarkable considering it possesses very low crystallinity (≤2% by DSC and WAXS), even after annealing at high temperature.[42] The chain solubility in boiling diethyl ether means that the overall tacticity must be low. Concurrently, the isotactic sequence lengths must also be sufficiently long to allow crystallization. From these observations, we conclude that ES cannot consist of a physical blend of isotactic and atactic chains owing to its low level of polydispersity ($M_w/M_n = 2.1$) and its solubility in ether. Rather, ES must consist of blocky microstructures with crystallizable isotactic and amorphous atactic segments chemically attached together.

Crystalline Form. The crystallization of the ES chains poses a question about the form of the crystalline phase formed. As stated previously, three crystalline forms are known in isotactic polypropylenes: α-, β-, and γ-form along with a mesomorphic crystalline form. WAXS data of stretched ES reveal scattering peaks corresponding to $2\theta = 16.0°$ ($d = 0.551 \pm 0.002$ nm). This coincides with the first crystalline peak of the β-form isotactic PP, suggesting that this form of the crystalline phase is formed.[2,3] However, the second characteristic peak of the β-form, with a weaker intensity, at $2\theta = 21.3°$ ($d = 0.417$ nm) is not observed in our system (Figures 6 and 7),[2,3] even at higher strains.

Previous literature in the field suggests an increased tendency to form β-form crystallites upon imposition of shear on isotactic polypropylenes.[2,3,53] Karger-Koscis et al. reported shear-induced crystallization of the β-form isotactic PP by stretching a glass fiber embedded in polypropylene matrix at 135 °C.[21−23] They revealed transcrystalline-like superstructures nucleated from the α-form row nuclei which could be selectively melted upon heating to 166 °C; the β-form crystallites possess a lower melting temperature than the α-form. The crystallization temperature and thermal stability of the

shear-induced crystallization reported by Karger-Kocsis et al. are different than those of the ES. The crystallites with orthogonally oriented chains in ES are observed at room temperature and completely melt near 75 °C, a much lower temperature than that observed by Karger-Kocsis and co-workers. Although other factors, such as highly defective crystal form, crystallization conditions, and heating rate, may affect the difference in the observed melting points, the crystallization of ES may have different origin and growth mechanism.

An investigation of the ES/HI blend and ePP provides insight into the role of the ES fraction under deformation when it is blended with crystallites of the α-form. As shown in Figures 8 and 9, the ES/HI blend reveals scattering peaks reminiscent of each fraction comprising the blend. It should be noted that scattering reflection corresponding to γ-form crystalline phase is not observed.[2] As mentioned previously, the arcing of ES/HI blend and ePP along the meridian occurs at $2\theta = 14.0°$ instead of at $2\theta = 16.0°$ as seen in the neat ES. The meridional arcing at the (110) scattering reflection of the α-form indicates a cocrystallization of the ES chains with the α-form crystallites. When ES is blended with the α-form crystallites, the ES crystallization follows the same crystalline form as the polymer host, by cocrystallizing with the higher-tacticity components.

The meridional arcing has also been observed previously on different studies of isotactic PP.[19] In the skin layer of injection-molded polypropylene, Fujiyama and co-workers showed the coexistence of the β-form with the matrix of the α-form.[54] The (100) β-form reflection was observed along the equatorial axis in coexistence with meridional arcing at the (110) reflection. Hsiao et al. also observed meridional arcing at $2\theta = 14°$ in a step-shear deformation at 150 °C,[55] similar to what we observed in our system. In addition, they also observed a reflection along the equator at $2\theta = 16°$, showing shear-induced crystallites of the β-form, similar to that reported by Fujiyama and co-workers. Kumaraswamy et al. also observed meridional arcing after a brief interval of shear at 141 °C but did not detect any β-form crystalline reflection at $2\theta = 16°$.[14] Compared to their systems, our results show interesting similarities and differences. We observed reflection only at $2\theta = 16.0°$ on the neat ES along the meridian axis. When ES is blended with crystallites of the α-form, the meridonal arcs appear at a lower scattering angle, at $2\theta = 14.0°$ corresponding to the (110) crystalline reflection of α-form, similar to what Kumaraswamy et al. observed.[14]

Crystalline Growth Model. Our results do not allow an unambiguous interpretation of the origin of the orthogonally oriented crystalline chains. The two mechanisms previously mentioned or their combination (crystalline lamellae reorientation and deformation-induced crystallization) can be used to interpret the observed negative birefringence and the meridional arcing. In the neat ES fraction, the lamellae that are already present in the material can simply be oriented in the presence of a stress field. Alternatively, the oriented lamellae may also act as nucleation sites to induce nucleation to cause deformation-induced crystallization.

Figure 11 contains a proposed crystalline growth model of the neat ES fraction. The model assumes that the observed orthogonally oriented crystalline chains arise from a combination of the lamellae reorientation and deformation-induced crystallization. As expected,
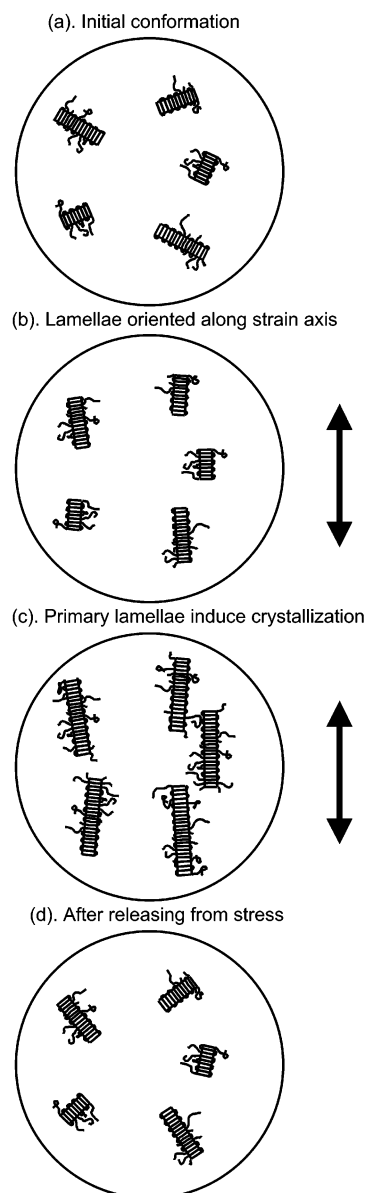

Figure 11. Schematic of a lamellae orientation and growth model of ES: (a) before deformation, lamellae are oriented isotropically; (b) deformation orients the lamellae along the strain axis; (c) oriented lamellae induce subsequent crystallization; and (d) when release from strain, the oriented lamellae are able to relax.

the crystalline lamella orientation could not be identified from small-angle X-ray scattering (SAXS) due to its low crystallinity. Deformation induces an orientation of the lamellae with long axis aligned with the deformation direction. The degree of orientation is dependent on several aspects such as lamellae mobility in the amorphous matrix, external deformation, and relaxation time. We believe that the aligned lamellae act as primary nuclei to induce crystallization. The induced crystallization grows from both ends of the oriented lamellae. Primary nucleation can be initiated if the helical arrangement of the crystallizable chains is correct, i.e., the left- and right-handed helices as well as "up" and "down" arrangement of the pending CH_3 group. Increasing deformation generates more oriented lamellae and thus a larger number of nucleation sites. Although lamellae are aligned preferentially along the strain direction, the chain-folding packing causes individual chains to align orthogonal relative to the strain
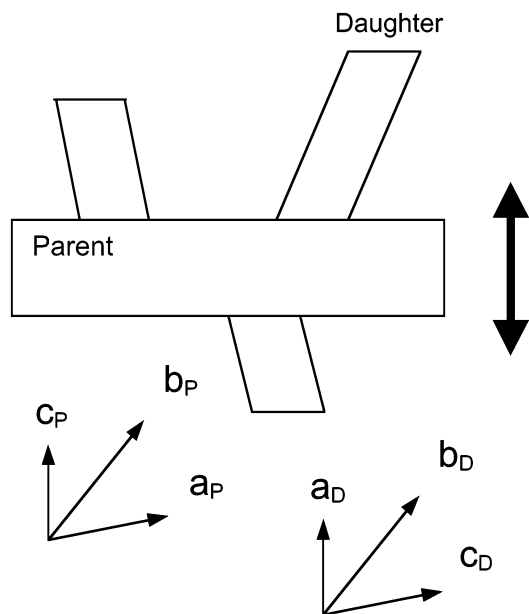
Figure 12. Schematic of a daughter lamellae growth model of ES in blends containing crystallites of the α-form.

direction. In a pure lamellae reorientation model, the induced crystallization simply does not occur. The orthogonally oriented chains conform to the observed negative birefringence and the WAXS meridional arcs. When ES is free from stress, the induced crystallization disappears due to the relaxation of the oriented lamellae toward an isotropic state.

In the blend of ES with higher-tacticity components, the observed crystallization can also be interpreted in terms of the two limiting cases. In one scenario, the ES chains cocrystallize with the α-form domains with the crystalline chain packed according to the (110) scattering reflection. Deformation causes the ES crystallites already present in the sample to align preferentially with the strain axis. In a different scenario, the ES chains undergo deformation-induced crystallization to cocrystallize with the α-form under strain. In this model, the observed crystallization occurs only when the material is under strain.

Padden et al.[55,56] and Lotz et al.[5,57,58] attributed the meridional arcing at $2\theta = 14°$ to epitaxy in the lateral *ac*-faces of the lateral plane (010) of the α-form. Daughter lamellae grow epitaxially with their *a*- and *c*-axes parallel to the *c*- and *a*-axes of the parent lamellae, respectively. The epitaxial growth is favored by a satisfactory interdigitation of the methyl groups of facing planes. The branching is initiated by the deposition of chains of the same handedness as chains in the lateral (010) face that is different than the α-form which favors opposite handedness of chains.

We believe the crystallization of ES in the presence of higher-tacticity components follows the same growth mechanism as described by Padden et al. and Lotz et al. The ES chains crystallize by growing epitaxially on the (010) lateral face with a normal edge-on lamellae growth on the parent lamellae (Figure 12). The parent lamellae, oriented orthogonal to the strain axis, act as nucleation sites. Under correct chain conformations (helical handedness and methyl side chain configuration), the ES chains can rearrange into epitaxially grown crystals almost perpendicular (80° or 100°) to the parent lamellae. Chains in the daughter lamellae are oriented such that the *a*- and *c*-axis are oriented parallel to the

c- and *a*-axis of the parent lamellae, respectively. Since the polymer chains are arranged in a chain-folded configuration, the chains in the crystals are aligned with a preferred orientation orthogonal to the strain axis, giving rise to the meridional arcing and negative birefringence.

The different crystalline growth mechanisms of the ES fraction when it is by itself and when it is blended with higher-tacticity fractions demonstrate the unusual properties of the low-tacticity fraction of the elastomeric PP. In the neat form, ES exhibits crystallinity of an unidentified crystalline form. When ES is present in crystallites of the α-form, the ES chains cocrystallize with the crystalline matrix through an epitaxial growth on the (010) lateral face of the α-form. Our results corroborate with the blocky microstructure model of alternating runs of isotactic and atactic sequences. The crystallization of the ES chains offers evidence that the distribution of isotactic sequences is long enough to cause crystallization. Moreover, although the meridional arcing has been observed previously, we have unambiguously shown that the low-tacticity ether-soluble fraction leads to an increase in meridional arcing. This finding will hopefully bring a better understanding of the crystal growth mechanism of polypropylenes.

Conclusions

The ether-soluble (ES) fraction of elastomeric polypropylene derived by bis(2-(3,5-di-*tert*-butylphenyl)indenyl)-hafnium dichloride catalyst shows unusual deformation properties as revealed by tensile stress, rheooptics birefringence, and X-ray scattering methods. Deformation causes the ES chains, crystallized within crystalline domains, to preferentially align orthogonal relative to the strain/shear direction. Two complementary methods, birefringence and WAXS, confirm the unusual crystalline chain orientation induced by deformation. The type of the crystalline form is not conclusively determined. Arcing along the meridian axis coincides with the strong scattering peak of the two characteristic reflections of the β-form ($2\theta = 16.0°$); however, the higher order reflection at $2\theta = 21.3°$ is not observed. The induced crystalline phase melts near 75 °C, a much lower temperature than the melting point of the β-form crystallites, which may be attributed to many factors including a highly defective crystal form, crystallization conditions, and heating rate. The crystallization of the low-crystallinity ES (≤2% by DSC and WAXS) implies there exist long crystallizable sequences to form crystallites. Concurrently, the solubility in boiling diethyl ether means the overall tacticity of the chains must be low, which suggests that the crystallizable sequences are covalently bonded to the highly soluble atactic sequences.

Crystallization of the low-tacticity fraction of ePP is also observed when ES is blended with crystallites of the α-form, as in ePP and in ES/HI blend. The crystallization, however, follows a different mechanism than in the neat ES. Meridional arcing occurs at the (110) reflections of the α-form, corresponding to $2\theta = 14.0°$ instead of at $2\theta = 16.0°$ seen in the neat ES. The crystallization in the same crystalline form as the matrix implies a cocrystallization between the ES fraction and the higher-crystallinity components. We believe that the cocrystallization follows a mechanism of daughter lamellae growth model on the (010) lateral face of the α-form crystallites. Daughter lamellae grow

epitaxially with their *a*- and *c*-axis parallel to the *c*- and *a*-axis of the parent lamellae, respectively. Our study has demonstrated the unusual deformation behavior of the low-tacticity ether-soluble fraction of elastomeric polypropylene.

References and Notes

(1) Ven, S. V. D. *Polypropylene and Other Polyolefins: Polymerization and Characterization*; Elsevier: New York, 1990.
(2) Karger-Kocsis, J. *Polypropylene: Structure, Blends and Composites*, 1st ed.; Chapman & Hall: New York, 1995.
(3) Moore, E. P. *Polypropylene Handbook: Polymerization, Characterization, Properties, Processing, Applications*; Hanser/Gardner Publications: New York, 1996.
(4) Natta, G.; Corradini, P. *Nuovo Cimento* **1960**, *15*, 40−51.
(5) Lotz, B.; Wittmann, J. C.; Lovinger, A. J. *Polymer* **1996**, *37*, 4979−4992.
(6) Meijer, H. E. H., Ed.; *Processing of Polymers*; VCH: New York, 1997; Vol. 18.
(7) Liedauer, S.; Eder, G.; Janeschitz-Kriegl, H.; Jerschow, P.; Geymayer, W.; Ingolic, E. *Int. Polym. Process.* **1993**, *8*, 236−244.
(8) Eder, G.; Janeschitz-Kriegl, H. In *Processing of Polymers*; VCH: New York, 1997; Vol. 18, pp 269−342.
(9) Keller, A.; Kolnaar, H. W. H. In *Processing of Polymers*; Meijer, H. E. H., Ed.; VCH: New York, 1997; Vol. 18, pp 189−268.
(10) Tribout, C.; Monasse, B.; Haudin, J. M. *Colloid Polym. Sci.* **1996**, *274*, 197−208.
(11) Jerschow, P.; Janeschitz-Kriegl, H. *Rheol. Acta* **1996**, *35*, 127−133.
(12) Monasse, B. *J. Mater. Sci.* **1995**, *30*, 5002−5012.
(13) Kumaraswamy, G.; Issaian, A. M.; Kornfield, J. A. *Macromolecules* **1999**, *32*, 7537−7547.
(14) Kumaraswamy, G.; Verma, R. K.; Issaian, A. M.; Wang, P.; Kornfield, J. A.; Yeh, F.; Hsiao, B. S.; Olley, R. H. *Polymer* **2000**, *41*, 8931−8940.
(15) Kumaraswamy, G.; Verma, R. K.; Kornfield, J. A. *Rev. Sci. Instrum.* **1999**, *70*, 2097−2104.
(16) Chu, B.; Hsiao, B. S. *Chem. Rev.* **2001**, *101*, 1727−1761.
(17) Ran, S. F.; Zong, X. H.; Fang, D. F.; Hsiao, B. S.; Chu, B.; Phillips, R. A. *Macromolecules* **2001**, *34*, 2569−2578.
(18) Somani, R. H.; Hsiao, B. S.; Nogales, A.; Fruitwala, H.; Srinivas, S.; Tsou, A. H. *Macromolecules* **2001**, *34*, 5902−5909.
(19) Nogales, A.; Hsiao, B. S.; Somani, R. H.; Srinivas, S.; Tsou, A. H.; Balta-Calleja, F. J.; Ezquerra, T. A. *Polymer* **2001**, *42*, 5247−5256.
(20) Wang, Z. G.; Hsiao, B. S.; Sirota, E. B.; Agarwal, P.; Srinivas, S. *Macromolecules* **2000**, *33*, 978−989.
(21) Varga, J.; Karger-Kocsis, J. *Polym. Bull. (Berlin)* **1993**, *30*, 105−110.
(22) Wu, C.-M.; Chen, M.; Karger-Kocsis, J. *Polymer* **1999**, *40*, 4195−4203.
(23) Wu, C.-M.; Chen, M.; Karger-Kocsis, J. *Polym. Bull. (Berlin)* **1998**, *41*, 493−499.
(24) Chen, R.; Xie, M. R.; Wu, Q.; Lin, S. G. *J. Polym. Sci., Part A: Polym. Chem.* **2000**, *38*, 411−415.
(25) Kuhl, O.; Koch, T.; Somoza, F. B.; Junk, P. C.; Hey-Hawkins, E.; Plat, D.; Eisen, M. S. *J. Organomet. Chem.* **2000**, *604*, 116−125.
(26) Longo, P.; Amendola, A. G.; Fortunato, E.; Boccia, A. C.; Zambelli, A. *Macromol. Rapid Commun.* **2001**, *22*, 339−344.
(27) Mansel, S.; Perez, E.; Benavente, R.; Perena, J. M.; Bello, A.; Roll, W.; Kirsten, R.; Beck, S.; Brintzinger, H. H. *Macromol. Chem. Phys.* **1999**, *200*, 1292−1297.
(28) Nedorezova, P. M.; Tsvetkova, V. I.; Bravaya, N. M.; Savinov, D. V.; Optov, V. A. *J. Polym. Sci., Ser. A* **2000**, *42*, 573−579.
(29) Schmidt, R.; Alt, H. G. *J. Organomet. Chem.* **2001**, *621*, 304−309.
(30) Yoon, J. S.; Lee, Y. S.; Park, E. S.; Lee, I. M.; Park, D. K.; Jung, S. O. *Eur. Polym. J.* **2000**, *36*, 1271−1275.
(31) Resconi, L.; Piemontesi, F.; Lin-Chen, Y. U.S. Patent 5,747,621, 1998.
(32) Sassmannshausen, J.; Bochmann, M.; Rosch, J.; Lilge, D. *J. Organomet. Chem.* **1997**, *548*, 23−28.
(33) Chien, J. C. W.; Iwamoto, Y.; Rausch, M. D.; Wedler, W.; Winter, H. H. *Macromolecules* **1997**, *30*, 3447−3458.
(34) Bravakis, A. M.; Bailey, L. E.; Pigeon, M.; Collins, S. *Macromolecules* **1998**, *31*, 1000−1009.
(35) Dietrich, U.; Hackmann, M.; Rieger, B.; Klinga, M.; Leskelae, M. *J. Am. Chem. Soc.* **1999**, *121*, 4348−4355.
(36) Kukral, J.; Lehmus, P.; Feifel, T.; Troll, C.; Rieger, B. *Organometallics* **2000**, *19*, 3767−3775.
(37) Pellon, B. J.; Allen, G. C. Eur. Pat. Appl. 0 475 306 A1, 1992.
(38) Coates, G. W.; Waymouth, R. M. *Science* **1995**, *267*, 217−219.
(39) Hu, Y. R.; Krejchi, M. T.; Shah, C. D.; Myers, C. L.; Waymouth, R. M. *Macromolecules* **1998**, *31*, 6908−6916.
(40) Kravchenko, R.; Masood, A.; Waymouth, R. M.; Myers, C. L. *J. Am. Chem. Soc.* **1998**, *120*, 2039−2046.
(41) Petoff, J. L. M.; Agoston, T.; Lal, T. K.; Waymouth, R. M. *J. Am. Chem. Soc.* **1998**, *120*, 11316−11322.
(42) Schonherr, H.; Wiyatno, W.; Pople, J. A.; Frank, C. W.; Fuller, G. G.; Gast, A. P.; Waymouth, R. M. *Macromolecules* **2002**, *35*, 8488−8497.
(43) Wiyatno, W.; Chen, Z.-R.; Liu, Y.; Waymouth, R. M.; Krukonis, V.; Brennan, K., submitted to *Macromolecules*.
(44) Bruce, M. D.; Coates, G. W.; Hauptman, E.; Waymouth, R. M.; Ziller, J. W. *J. Am. Chem. Soc.* **1997**, *119*, 11174−11182.
(45) Fuller, G. G. *Optical Rheometry of Complex Fluids*; Oxford University Press: New York, 1995.
(46) Janeschitz-Kriegl, H. *Polymer Melt Rheology and Flow Birefringence*; Springer-Verlag: Berlin, 1983.
(47) Wales, J. L. S. *The Application of Flow Birefringence to Rheological Studies of Polymer Melts*; Delft University Press: Delft, 1976.
(48) Macosko, C. W.; Larson, R. G. *Rheology: Principles, Measurements, and Applications*; VCH: New York, 1994.
(49) Gomez, M. A.; Tanaka, H.; Tonelli, A. E. *Polymer* **1987**, *28*, 2227−2232.
(50) Corradini, P.; Derosa, C.; Guerra, G.; Petraccone, V. *Polym. Commun.* **1989**, *30*, 281−285.
(51) Martorana, A.; Piccarolo, S.; Scichilone, F. *Macromol. Chem. Phys.* **1997**, *198*, 597−604.
(52) Kravchenko, R. L.; Sauer, B. B.; McLean, R. S.; Keating, M. Y.; Cotts, P. M.; Kim, Y. H. *Macromolecules* **2000**, *33*, 11−13.
(53) Wenig, W.; Herzog, F. *J. Appl. Polym. Sci.* **1993**, *50*, 2163−2171.
(54) Fujiyama, M.; Wakino, T.; Kawasaki, Y. *J. Appl. Polym. Sci.* **1988**, *35*, 29−49.
(55) Padden, F. J., Jr.; Keith, H. D. *J. Appl. Phys.* **1973**, *44*, 1217−1223.
(56) Padden, F. J., Jr.; Keith, H. D. *J. Appl. Phys.* **1966**, *37*, 4013−4020.
(57) Wittmann, J. C.; Lotz, B. *Prog. Polym. Sci.* **1990**, *15*, 909−948.
(58) Lotz, B.; Wittmann, J. C. *J. Polym. Sci., Part B: Polym. Phys.* **1986**, *24*, 1514−1558.

MA020262G